Support information

Thalia dealbata-inspired Anisotropic Cellular Biomass-derived Carbonaceous Aerogel

Tao Chen [a,b], Jian Zhang [a], Peiheng Shi [b], Yi Li [a], Ling Zhang [a, b], Zhengzong Sun [c], Rong He [a, b], Tao Duan [a,b]*, Wenkun Zhu [a, b, d]*

[a] *State Key Laboratory of Environmentally Friendly Energy Materials and Biomass Materials, Southwest University of Science and Technolog, No. 59 Qinglong Avenue, Fucheng district, Mianyang, Sichuan, 621010, P. R. China.*

[b] *Nuclear Waste and Environmental Safety Key Laboratory of Defense, Southwest University of Science and Technology, No. 59 Qinglong Avenue, Fucheng district, Mianyang, Sichuan, 621010, P. R. China.*

[c] *Department of Chemistry and Shanghai Key Laboratory of Molecular Catalysis and Innovative Materials, Fudan University, Shanghai, 200433, P. R. China.*

[d] *University of Science and Technology of China, Anhui Hefei 230026, P. R. China.*

*. *Corresponding Author, E-mail: zhuwenkun@swust.edu.cn (Wenkun Zhu); duant@ustc.edu.cn (Tao Duan).*

Author E-mail: 18181748525@163.com (Tao Chen), 2358727542@qq.com (Jian Zhang), 1124586052@qq.com (Peiheng Shi), liyi012315@163.com (Yi Li), zhangling860817@163.com (Ling Zhang), zhengzong_sun@fudan.edu.cn (Zhengzong Sun), her@mail.ustc.edu.cn (Rong He).

Supporting information is a total of 14 pages

Electrochemical measurements

All electrochemical tests were performed on a CHI 760D electrochemical workstation with a three-electrode test system using platinum sheet electrode as counter electrode, as-prepared active material modified electrode as working electrode referred to Hg/HgO electrode in 1.0 M KOH. The cyclic voltammetry (CV) curve was obtained at a scan speed of 5-100 mV/s at an operating voltage of -1.0-0 V relative to Hg/HgO electrode. The galvanostatic charge-discharge (GCD) test was carried out at a current density of 1-20 A g^{-1} and a voltage of -1.0-0 V relative to the Hg/HgO electrode. In addition, electrochemical impedance spectroscopy (EIS) was measured an open circuit voltage in the frequency range from 1 MHz to 0.01 Hz with an amplitude of 5 mV. The working electrode was prepared as follows: first, 80 wt % of the active material, 10 wt % of carbon black and 10 wt % of polytetrafluoroethylene (dispersed in N-methylpyrrolidone) were mixed together and ground to a slurry. The slurry was then supported on foam nickel and dried under vacuum at 60 °C for 5 h. Next, the electrode was pressed at a pressure of 10 MPa and then dried in a vacuum oven at 100 °C for 12 h. The area of the electrode was 1.0 cm^2, and the amount of active material loaded on each collector was 5.0-6.0 mg.

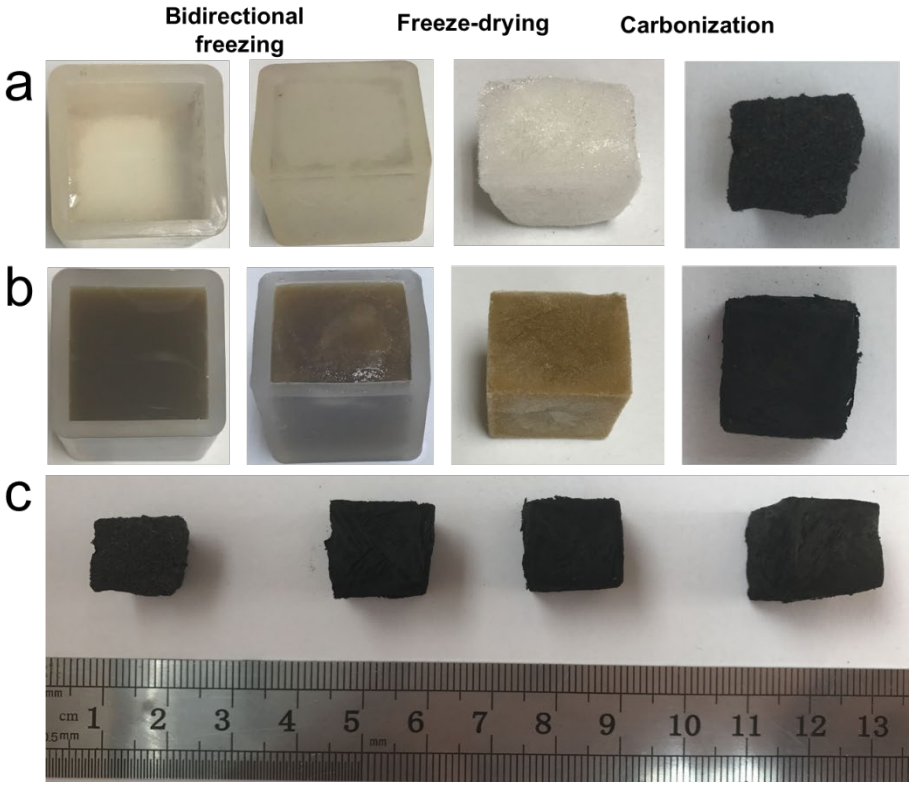

Figure S1. (a,b)Digital photographs show the fabrication process of unique hierarchical mineral bridge structured KA and KGA, (c) Digital photographs of KGA with different concentrations of GO.

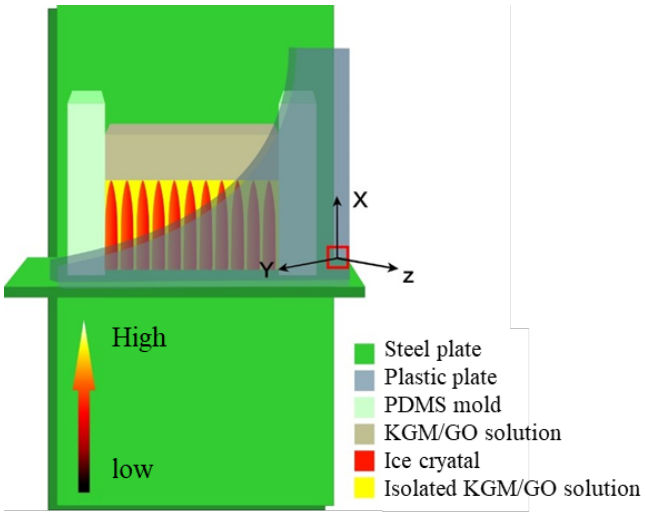

Figure S2. Schematic illustrations of bidirectional freezing. In a typical freeze-casting process, the KGM/GO mixture suspension was poured into a cubic silicone mould, which was placed on a cold stainless steel plate that was pro-cooled by liquid nitrogen. Therefore, the temperature of the cold stainless steel plate was far below the freezing point of the mixture suspension. Because the thermal conductivity of the silicone mould is much lower than that of cold stainless steel plate, the ice crystals would mainly grow from bottom to top in the KGM/GO mixture suspension when it was contacted to the cold stainless steel plate. In the freeze-casting process, ice crystals grew from bottom to top, expelled the KGM/GO mixture suspension to the boundaries between ice

crystals and resulted in a directional hierarchical 3D structure.

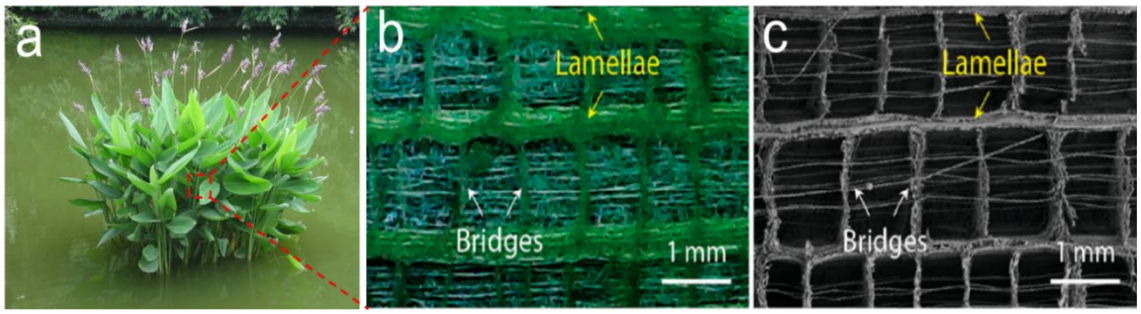

Figure S3. (a) Optical image of a Thalia dealbata. (b and c)Optical and SEM images showing themultiscale architecture. b and c) come from the literature[1].

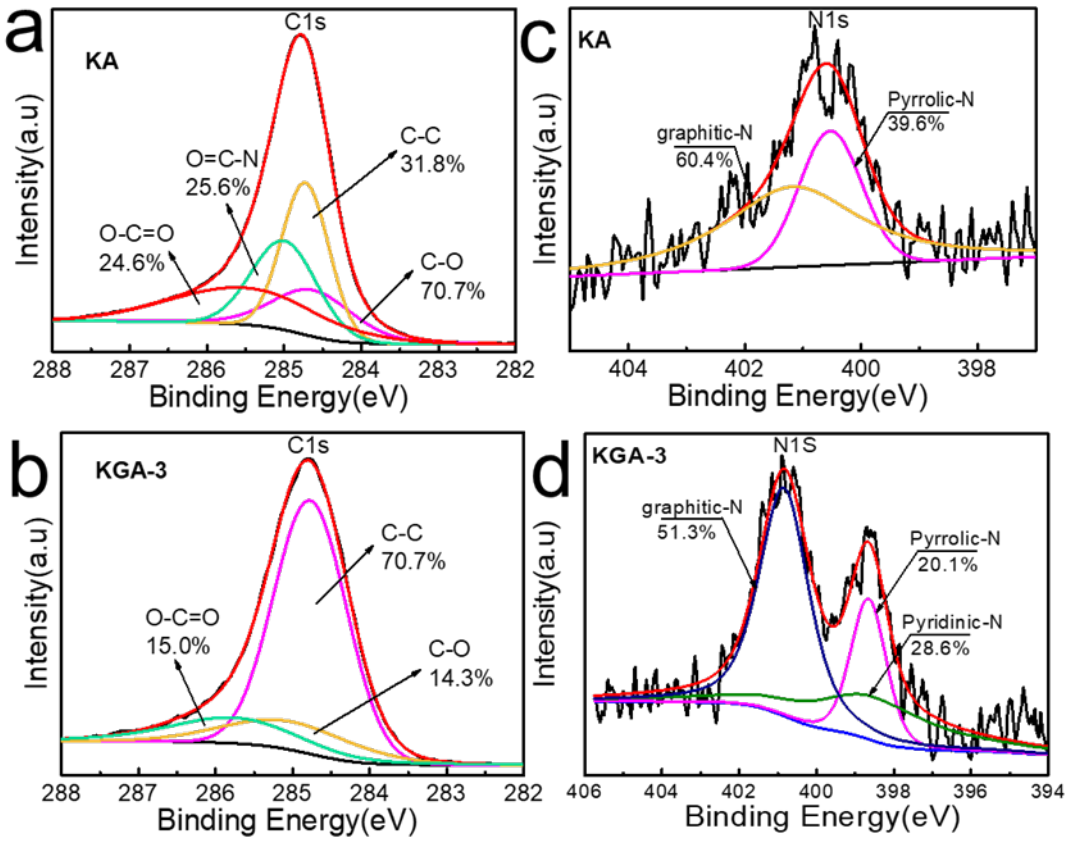

Figure S4. High resolution XPS spectra of C1s (a, b) and N1s (c, d).

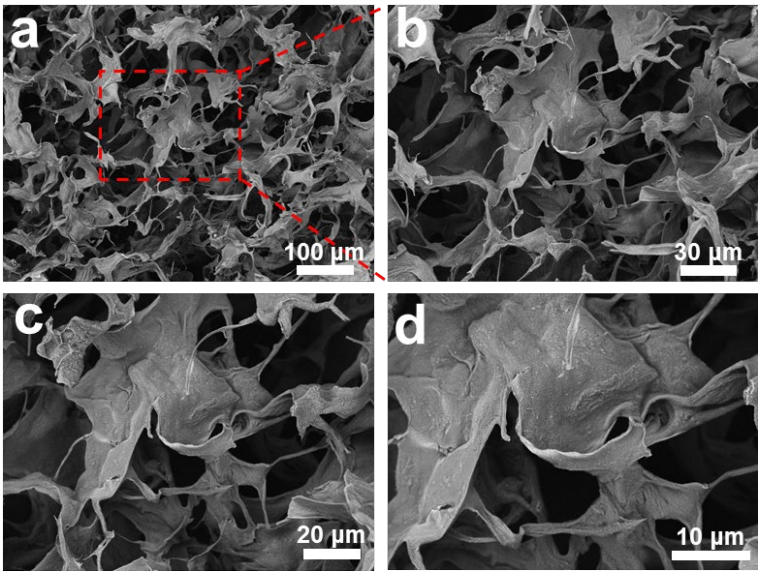

Figure S5.SEM images of 3D network structure of KGA-3 (disordered).

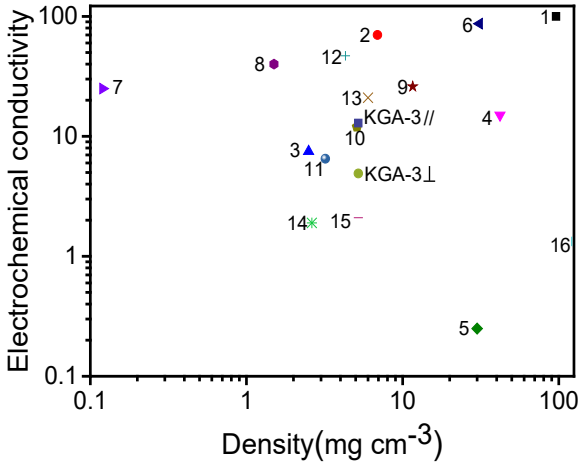

Figure S6.Comparison of the electrical conductivity of unique mineral bridge structured KGA-3 as a function of density to the several previously reported low-density carbon aerogels[2-17].

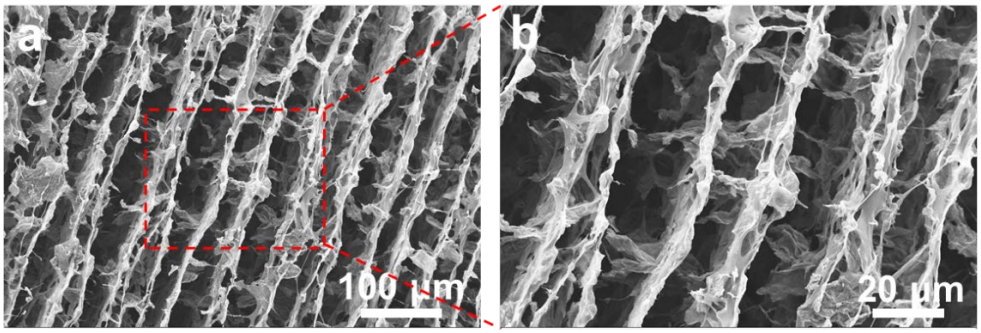

Figure S7. SEM of KGA-3 after 80% compression recovery.

KGA is used as a supercapacitor.

In addition to flexible piezoresistive sensors, KGA can also be used as a supercapacitors. To discuss the electrochemical performances of obtained KGA-3 in a three-electrode system in 1.0 M KOH electrolyte. Figure S8a show the CV curves of KGA-3 at various scan rates ranging from 5 to 50 mV/s in the potential range of -1.0 to 0 V. With the increasing sweep speed, the CVs exhibited no significant changes and maintained a clear rectangle, even at 50 mV s^{-1}, thus showing that the KGA-3 had a good rate performance. The capacitance performance was verified by the GCD profiles under different current densities. The specific capacitance for KGA-3 electrode is 287.6 F/g at the current density of 20 A/g, consistent with the CV results (Figure S8b). Compared with other materials, KGA-3 has a higher specific capacitance. This is mainly due to the higher larger specific surface area and nitrogen doping, which can change the electronic properties of carbon nanosheets and facilitate the transfer of electrolyte ions into the interior of carbon material. Surprisingly, its capacitance was still 129.4 F g^{-1} at this current density of 1 A/g, which corresponds to capacity retention of approximately 44.993% and shows the excellent rate performance (Figure S8c).

Electrochemical impedance spectroscopy (EIS) is a powerful means of studying the resistance between the electrolyte and the electrode and the internal resistance of the electrode[18]. Figure S8d shows the Nyquist plots of KGA-3 in the frequency range from 0.01 Hz to 1 MHz. Nyquist plots are consisted of a straight line in the low frequency region a semicircle and in the high frequency region[19]. The KGA-3 had a unique layered structure and high specific surface area, which promoted the transport and migration of ions in the electrolyte to enhance electrochemical performance[18]. In addition, the stability of KGA-3 was also tested by LSV (Figure S9), because durability is also an important aspect of electrochemical performance. It can be observed that there was only a slight decrease (1.7 %) in the activity of the KGA-3 in the 600 cycle test, this result shows that KGA-3 has good electrocatalytic stability.

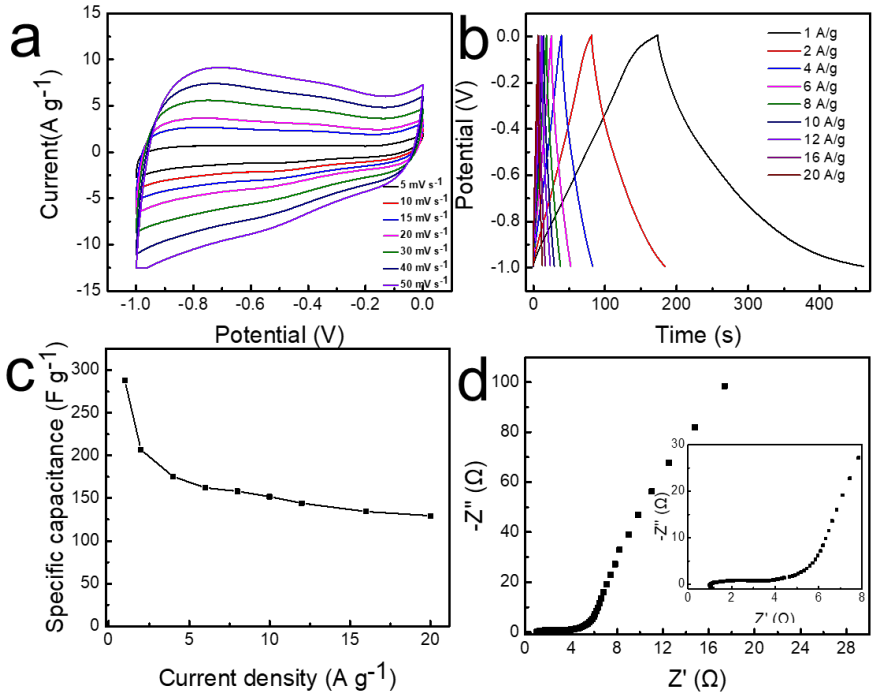

137

138 **Figure S8**.Electrochemical performances of KGA-3 measured in a three-electrode
139 system. (a) CV curves of KGA-3 at different scan rates; (b) GCD profiles of KGA-3 at
140 various current densities; (c) Specific capacitances of KGA-3 at different current
141 densities; (e) Nyquist plots of KGA-3 in 1.0 M KOH in a frequency range from 1 MHz
142 to 0.01 Hz.

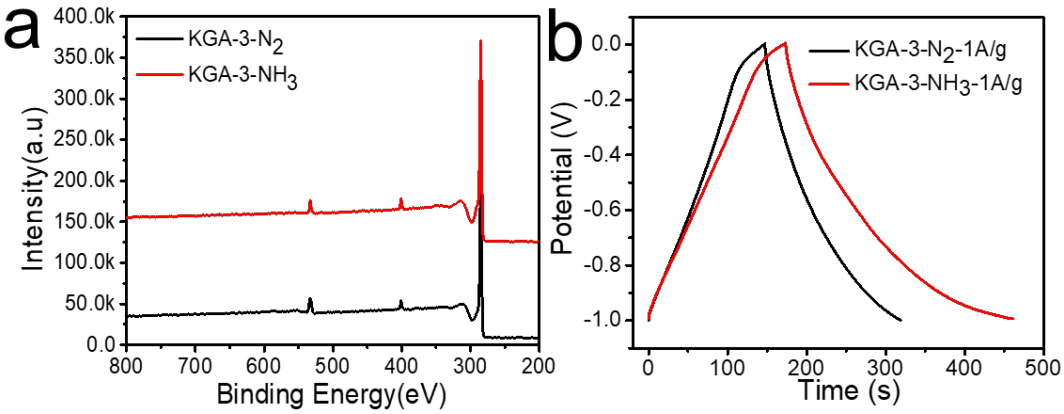

143

144 **Figure S9**. (a)XPS spectra of KGA-3-N_2 and KGA-3-NH_3. (b) GCD profiles of KGA-
145 3-N_2 and KGA-3-NH_3 at this current density of 1 A/g.

146

147

148

Table S1. The contents of C, O and N obtained by XPS in KGA-3.

Groups	C (%)	O (%)	N (%)
KGA-3-N_2	80.4	12.9	6.7
KGA-3-NH_4	80.9	10.5	8.6

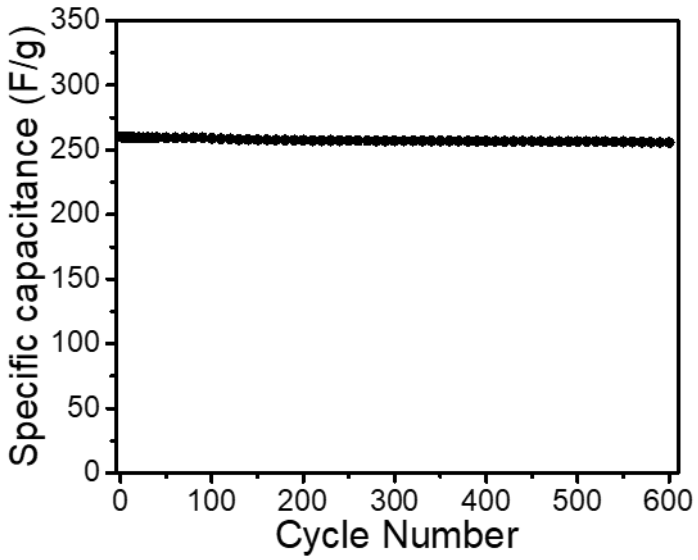

Figure S10.Cycling performance of the KGA-3.

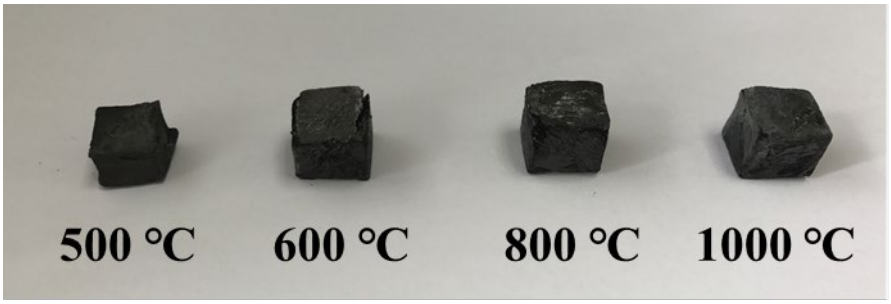

Figure S11.Digital photographs of KGA-3 with different carbonization temperatures.

Figure S12. Digital photographs of KGA-3 compression test with a carbonization temperature of 800 °C.

Table S2. Building blocks, preparation methods, density, compressibility, adsorption capacity of previously reported 3D materials and the KGAs in this work.

Sample name	Building blocks	Preparation methods	Density (mg/cm^3)	Compressibility (%)	Cost	Ref
WCA	Winter melon	Hydrothermal freeze-drying pyrolysis	48	-	Low	[20]
CMB aerogel	Waste paper	Freeze-drying	5.8	-	Low	[21]
TCF aerogel	Cotton	Pyrolysis	12	-	Low	[22]
CNF aerogel	Bacterial cellulose	Freeze-drying pyrolysis	4-6	90	Low	[23]
Nanocellulose aerogel	Cellulose nanofibril	Freeze-drying	20-30	-	Low	[24]
PSC aerogel	Bacterial cellulose poplars catkin	Hydrothermal freeze-drying pyrolysis	4.3	80	Low	[25]
S-PPy/RGO aerogel	GO	Hydrothermal	140		High	[26]
Spongy graphene	GO	Hydrothermal freeze-drying	12	-	High	[27]
NGA	GO	Hydrothermal pyrolysis	1.9	-	High	[28]
GA	GO	Chemical reduction freeze-drying	5	80	High	[29]
CNT spongy	CNTs	Chemical vapor deposition	10-29	60	High	[30]
CNT spongy	CNTs	Chemical vapor deposition	5-10	80	High	[31]
UFA	GO+CNTs	Freeze-drying Chemical reduction	0.16	50	High	[14]

Graphene/CNT foam	GO+CNTs	Chemical vapor deposition	6.92		High	[32]
PU spongy	PU	Dip-coating	-	-	Medium	[33]
PU spongy	PU	Dip-coating	-	80	Medium	[34]
CS-sponge	Melamine sponge	Dip-coating	30	-	Medium	[35]
Silanized Melamine Sponge	Melamine Sponge	Dip-coating	4-12	-	Medium	[36]
PDMS sponge	Organic siloxane	Templating Sol-gel	-	90	Medium	[37]
Marshmallow-like gel	Organic siloxane	Sol-gel	120	80	High	[38]
BSQ aerogel	Organic siloxane	Sol-gel	55-83	50	High	[39]
KGA	KGM/GO	Freeze-casting freeze-drying carbonization	4.2-11.2	80	Medium	This work

References

(1) Yang, M.; Zhao, N.; Cui, Y.; Gao, W.; Zhao, Q.; Gao, C.; Bai, H.; Xie, T. Biomimetic Architectured Graphene Aerogel with Exceptional Strength and Resilience. *Acs Nano* **2017,** *11* (7), 6817.

(2) Zhang, X.; Sui, Z.; Xu, B.; Yue, S.; Luo, Y.; Zhan, W.; Liu, B. Mechanically strong and highly conductive graphene aerogel and its use as electrodes for electrochemical power sources. *Journal of Materials Chemistry* **2011,** *21* (18), 6494-6497.

(3) Zhang, X.; Liu, J.; Xu, B.; Su, Y.; Luo, Y. Ultralight conducting polymer/carbon nanotube composite aerogels. *Carbon* **2011,** *49* (6), 1884-1893.

(4) Sui, Z.; Meng, Q.; Zhang, X.; Ma, R.; Cao, B. Green synthesis of carbon nanotube–graphene hybrid aerogels and their use as versatile agents for water purification. *Journal of Materials Chemistry* **2012,** *22* (18), 8767-8771.

(5) Chen, W.; Li, S.; Chen, C.; Yan, L. Self-assembly and embedding of nanoparticles by in situ reduced graphene for preparation of a 3D graphene/nanoparticle aerogel. *Advanced Materials* **2011,** *23* (47), 5679-5683.

(6) Tang, Z.; Shen, S.; Zhuang, J.; Wang, X. Noble-metal-promoted three-dimensional macroassembly of single-layered graphene oxide. *Angewandte Chemie* **2010,** *122* (27), 4707-4711.

(7) Zhu, C.; Han, Y. J.; Duoss, E. B.; Golobic, A. M.; Kuntz, J. D.; Spadaccini, C. M.; Worsley, M. A. Highly compressible 3D periodic graphene aerogel microlattices. *Nature Communications* **2015,** *6*, 6962.
(8) Si, Y.; Yu, J.; Tang, X.; Ge, J.; Ding, B. Ultralight nanofibre-assembled cellular aerogels with superelasticity and multifunctionality. *Nature Communications* **2014,** *5*, 5802.
(9) Barg, S.; Perez, F. M.; Ni, N.; Pereira, P. D. V.; Maher, R. C.; Garciatuñon, E.; Eslava, S.; Agnoli, S.; Mattevi, C.; Saiz, E. Mesoscale assembly of chemically modified graphene into complex cellular networks. *Nature Communications* **2014,** *5*, 4328.
(10) Zou, J.; Liu, J.; Karakoti, A. S.; Kumar, A.; Joung, D.; Li, Q.; Khondaker, S. I.; Seal, S.; Zhai, L. Ultralight Multiwalled Carbon Nanotube Aerogel. *Acs Nano* **2010,** *4* (12), 7293-7302.
(11) Qiu, L.; Liu, J. Z.; Chang, S. L.; Wu, Y.; Li, D. Biomimetic superelastic graphene-based cellular monoliths. *Nature Communications* **2012,** *3* (4), 1241.
(12) Qian, Y.; Ismail, I. M.; Stein, A. Ultralight, high-surface-area, multifunctional graphene-based aerogels from self-assembly of graphene oxide and resol. *Carbon* **2014,** *68* (3), 221-231.
(13) Li, L.; Tao, H.; Sun, H.; Zhang, J.; Wang, A. Pressure-Sensitive and Conductive Carbon Aerogels from Poplars Catkins for Selective Oil Absorption and Oil/Water Separation. *Acs Appl Mater Interfaces* **2017,** *9* (21), 18001-18007.
(14) Sun, H.; Xu, Z.; Gao, C. Multifunctional, ultra-flyweight, synergistically assembled carbon aerogels. *Advanced Materials* **2013,** *25* (18), 2554-2560.
(15) Wu, Z. Y.; Li, C.; Liang, H. W.; Chen, J. F.; Yu, S. H. Ultralight, Flexible, and Fire-Resistant Carbon Nanofiber Aerogels from Bacterial Cellulose. *Angewandte Chemie* **2013,** *52* (10), 2925-9.
(16) Si, Y.; Wang, X.; Yan, C.; Yang, L.; Yu, J.; Ding, B. Ultralight Biomass-Derived Carbonaceous Nanofibrous Aerogels with Superelasticity and High Pressure-Sensitivity. *Advanced Materials* **2016,** *28* (43), 9655-9655.
(17) Li, Y. Q.; Samad, Y. A.; Polychronopoulou, K.; Liao, K. Lightweight and Highly Conductive Aerogel-like Carbon from Sugarcane with Superior Mechanical and EMI Shielding Properties. *Acs Sustainable Chemistry & Engineering* **2015,** *3* (7), 150513102130001.
(18) Meng, Q.; Wan, H.; Zhu, W.; Duan, T.; Yao, W. Naturally Dried, Double Nitrogen-Doped 3D Graphene Aerogels Modified by Plant Extracts for Multifunctional Applications. *Acs Sustainable Chemistry & Engineering* **2018,** *6* (1), 1172-1181, DOI: 10.1021/acssuschemeng.7b03460.
(19) Lei, J.; Guo, Q.; Yao, W.; Duan, T.; Chen, P.; Zhu, W. Bioconcentration of organic dyes via fungal hyphae and their derived carbon fibers for supercapacitors. *Journal of Materials Chemistry A* **2018**, DOI: 10.1039/C8TA02655F.
(20) Li, Y. Q.; Samad, Y. A.; Polychronopoulou, K.; Alhassan, S. M.; Liao, K. Carbon Aerogel from Winter Melon for Highly Efficient and Recyclable Oils and Organic Solvents Absorption. *Acs Sustainable Chemistry & Engineering* **2014,** *2* (6), 1492-1497.
(21) Bi, H.; Huang, X.; Wu, X.; Cao, X.; Tan, C.; Yin, Z.; Lu, X.; Sun, L.; Zhang, H. Carbon microbelt aerogel prepared by waste paper: an efficient and recyclable sorbent

for oils and organic solvents. *Small* **2014,** *10* (17), 3544-3550.
(22) Bi, H.; Yin, Z.; Cao, X.; Xie, X.; Tan, C.; Huang, X.; Chen, B.; Chen, F.; Yang, Q.; Bu, X. Carbon fiber aerogel made from raw cotton: a novel, efficient and recyclable sorbent for oils and organic solvents. *Advanced Materials* **2013,** *25* (41), 5916.
(23) Wu, Z. Y.; Li, C.; Liang, H. W.; Chen, J. F.; Yu, S. H. Ultralight, flexible, and fire-resistant carbon nanofiber aerogels from bacterial cellulose. *Angewandte Chemie International Edition* **2013,** *52* (10), 3035-3035.
(24) Korhonen, J. T.; Kettunen, M.; Ras, R. H.; Ikkala, O. Hydrophobic nanocellulose aerogels as floating, sustainable, reusable, and recyclable oil absorbents. *Acs Applied Materials & Interfaces* **2011,** *3* (6), 1813.
(25) Li, L.; Hu, T.; Sun, H.; Zhang, J.; Wang, A. Pressure-Sensitive and Conductive Carbon Aerogels from Poplars Catkins for Selective Oil Absorption and Oil/Water Separation. *Acs Appl Mater Interfaces* **2017,** *9* (21), 18001-18007.
(26) Wu, F.; Xie, A.; Sun, M.; Wang, Y.; Wang, M. Reduced Graphene Oxide (RGO) Modified Sponge-like Polypyrrole (PPy) Aerogel for Excellent Electromagnetic Absorption. *Journal of Materials Chemistry A* **2015,** *3* (27), 14358-14369.
(27) Bi, H.; Xie, X.; Yin, K.; Zhou, Y.; Wan, S.; He, L.; Xu, F.; Banhart, F.; Sun, L.; Ruoff, R. S. Graphene: Spongy Graphene as a Highly Efficient and Recyclable Sorbent for Oils and Organic Solvents (Adv. Funct. Mater. 21/2012). *European Journal of Inorganic Chemistry* **2012,** *22* (21), 4421-4425.
(28) Song, X.; Lin, L.; Rong, M.; Wang, Y.; Xie, Z.; Chen, X. Mussel-inspired, ultralight, multifunctional 3D nitrogen-doped graphene aerogel. *Carbon* **2014,** *80* (1), 174-182.
(29) Xu, L.; Xiao, G.; Chen, C.; Li, R.; Mai, Y.; Sun, G.; Yan, D. Superhydrophobic and superoleophilic graphene aerogel prepared by facile chemical reduction. *Journal of Materials Chemistry A* **2015,** *3* (14), 7498-7504.
(30) Hashim, D. P.; Narayanan, N. T.; Romoherrera, J. M.; Cullen, D. A.; Hahm, M. G.; Lezzi, P.; Suttle, J. R.; Kelkhoff, D.; Muñozsandoval, E.; Ganguli, S. Covalently bonded three-dimensional carbon nanotube solids via boron induced nanojunctions. *Scientific Reports* **2012,** *2* (4), 363.
(31) Gui, X.; Wei, J.; Wang, K.; Cao, A.; Zhu, H.; Jia, Y.; Shu, Q.; Wu, D. Carbon nanotube sponges. *Advanced Materials* **2010,** *22* (5), 617.
(32) Dong, X.; Chen, J.; Ma, Y.; Wang, J.; Chan-Park, M. B.; Liu, X.; Wang, L.; Huang, W.; Chen, P. Superhydrophobic and superoleophilic hybrid foam of graphene and carbon nanotube for selective removal of oils or organic solvents from the surface of water. *Chemical Communications* **2012,** *48* (86), 10660.
(33) Wang, C. F.; Lin, S. J. Robust superhydrophobic/superoleophilic sponge for effective continuous absorption and expulsion of oil pollutants from water. *Acs Applied Materials & Interfaces* **2013,** *5* (18), 8861.
(34) Yang, Y.; Tong, Z.; Ngai, T.; Wang, C. Nitrogen-rich and fire-resistant carbon aerogels for the removal of oil contaminants from water. *Acs Appl Mater Interfaces* **2014,** *6* (9), 6351-6360.
(35) Gao, Y.; Zhou, Y. S.; Xiong, W.; Wang, M.; Fan, L.; Rabieegolgir, H.; Jiang, L.; Hou, W.; Huang, X.; Jiang, L. Highly Efficient and Recyclable Carbon Soot Sponge for

Oil Cleanup. *Acs Applied Materials & Interfaces* **2014,** *6* (8), 5924-5929.
(36) Pham, V. H.; Dickerson, J. H. Superhydrophobic silanized melamine sponges as high efficiency oil absorbent materials. *Acs Applied Materials & Interfaces* **2014,** *6* (16), 14181.
(37) Xia, Z.; Li, L.; Li, B.; Zhang, J.; Wang, A. Durable superhydrophobic/superoleophilic PDMS sponges and their applications in selective oil absorption and in plugging oil leakages. *Journal of Materials Chemistry A* **2014,** *2* (43), 18281-18287.
(38) Hayase, G.; Kanamori, K.; Fukuchi, M.; Kaji, H.; Nakanishi, K. Facile Synthesis of Marshmallow-like Macroporous Gels Usable under Harsh Conditions for the Separation of Oil and Water. *Angewandte Chemie International Edition* **2013,** *52* (7), 1986-1989.
(39) Wang, Z.; Wang, D.; Qian, Z.; Guo, J.; Dong, H.; Zhao, N.; Xu, J. Robust Superhydrophobic Bridged Silsesquioxane Aerogels with Tunable Performances and Their Applications. *Acs Applied Materials & Interfaces* **2015,** *7* (3), 2016-24.